TECHNICAL MEMORANDUM

358

Use of potential vorticity as a control variable within a 4D variational data assimilation system

M.J.P. Cullen

Research Department

Submitted for publication in Q. J. Roy. Met. Soc.

January 2002

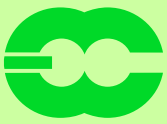

European Centre for Medium-Range Weather Forecasts
Europäisches Zentrum für mittelfristige Wettervorhersage
Centre européen pour les prévisions météorologiques à moyen terme

For additional copies please contact

The Library
ECMWF
Shinfield Park
Reading
RG2 9AX
library@ecmwf.int

Series: ECMWF Technical Memoranda

A full list of ECMWF Publications can be found on our web site under:
http://www.ecmwf.int/pressroom/publications/

Abstract

All variational data assimilation schemes use some form of mass-wind coupling in their definitions of the control variables used in the minimisation of the cost function. At ECMWF, the statistical coupling developed by Parrish and Derber (1992) is used. This is simple and robust. However, this robustness is obtained by assuming that the vorticity always represents balanced motion, and that balanced temperatures and pressures can be calculated from it.

On scales larger than the Rossby deformation radius, the temperature is more correctly used as the balanced variable. Use of potential vorticity, rather than vorticity, allows the correct choice of variable on all scales. A simple potential vorticity based method is developed and tested. It is shown that the strong scale dependence of the gravity wave speed introduces significant difficulties with this approach. However, with care, good results can be obtained.

1 Introduction

Many operational centres have now introduced variational methods of data assimilation. The work described in this paper is a development within the four-dimensional variational data assimilation (4D-VAR) system used operationally at ECMWF, Rabier et al. (2000). In common with other implementations of variational data assimilation, measures are taken to enforce a coupling between mass and wind increments in the minimisation step. The method used at ECMWF is described by Bouttier et al. (1997), and is very similar to that developed by Parrish and Derber (1992) and used in the NCEP operational system.

The operational method achieves simplicity and robustness by regarding the vorticity increments as the balanced increments, and computing height and hence temperature and surface pressure increments from them using a form of inverse balance equation. This is always easy to solve, as it requires only inversion of a Laplacian operator. The conversion from height to temperature and pressure increments is difficult because of the existence of a 'zero mode' where non-zero surface pressure and temperature increments can combine to give a zero height increment. Parrish and Derber developed a statistical procedure to avoid this problem, and also achieve appropriate couplings to the divergence increments.

According to standard geostrophic adjustment theory, the treatment of vorticity increments as balanced is appropriate on scales smaller than the Rossby radius of deformation. On larger scales, the mass increments determine the balanced response. Both regimes can be explained by making a change of variables to the potential vorticity and geostrophic departure, rather than vorticity and geopotential height. The solution to the geostrophic adjustment problem is then to preserve the potential vorticity, while setting the geostrophic departure to zero. It is thus natural to suggest that this change of variables should be used within the data assimilation.

In this paper we develop such a formulation. We show that there are difficulties on scales where the gravity wave speed is small and the change of variable formula very ill-conditioned. We show how this problem can be reduced by making an appropriate choice of control variable. However, the method is still impracticable using the operational vertical finite-difference scheme which, as well has having a 'zero mode', reduces the speed of the higher internal gravity wave modes substantially. It is possible to use the method with an experimental finite-element vertical discretisation developed by Untch and Hortal (2002), which increases the speed of the higher internal modes.

In the later sections of the paper we illustrate the effect of the change of variable by calculating various diagnostics from data sets of forecast errors. We then illustrate the performance within the ECMWF 4D-VAR system. This shows that the scheme gives much smoother wind analyses and better wind forecasts in the tropics. There is a noticeable impact on overall forecast performance.

2 The potential vorticity transformation

The change of variables used in the ECMWF data assimilation forms part of the inner minimisation loop and is performed in spectral space. The potential vorticity formulation for increments to the model variables has thus to take the form of a linear transformation, and it is necessary to assume a background state which depends only on pressure. In order to ensure consistency with the model dynamics, the change of variable uses the same background state as the semi-implicit integration scheme. However, it would also be possible to use a more accurate reference temperature, since the computational stability requirements that dictate the use of a very warm reference temperature are not relevant to the change of variable.

Following Simmons and Temperton (1997) and Temperton (1997), the linearised equations for a single zonal wavenumber can be written

$$\begin{aligned} \frac{\partial \zeta}{\partial t} + \mathbf{F}D &= \mathcal{Z} \\ \frac{\partial T}{\partial t} + \tau_r D &= \mathcal{T} \\ \frac{\ln p_{surf}}{\partial t} + \nu_{\mathbf{r}} D &= \mathcal{P} \\ \frac{\partial D}{\partial t} + \nabla^2(\gamma_r T + \sigma_r \ln p_{surf}) - \mathbf{F}\zeta &= \mathcal{D}. \end{aligned} \tag{1}$$

Here ζ is the vertical component of vorticity, D the horizontal divergence, T the temperature and p_{surf} the surface pressure. The other Greek letters denote matrices of values at model levels. $\mathbf{F}$ is a matrix connecting values at different meridional wavenumbers. The caligraphic letters represent the nonlinear terms and physical forcing. The suffixes r on the matrices indicates that they are derived from a reference state. No reference state quantities appear in $\mathbf{F}$. Equations (1) can be used to derive a second order equation for the divergence of the form

$$\frac{\partial^2 D}{\partial t^2} - \left(\nabla^2(\gamma_r \tau_r + \sigma_r \nu_{\mathbf{r}} + \mathbf{F}^2\right) D = \mathcal{G} \tag{2}$$

$\mathcal{G}$ represents a combination of the forcing terms $\mathcal{Z}, P, D$ and $\mathcal{T}$. This is an equation for forced inertio-gravity waves. It can be analysed by multiplying by the eigenvectors E_n of the matrix $\mathbf{B} = \gamma_r \tau_r + \sigma_r \nu$, giving

$$\frac{\partial^2 D_n}{\partial t^2} - \left(\nabla^2 c_n^2 + \mathbf{F}^2\right) D_n = \mathcal{G}_n \tag{3}$$

c_n is the gravity wave speed associated with the nth eigenvector. If we now multiply (3) by the eigenvectors of the horizontal operator $L = \nabla^2 c_n^2 + \mathbf{F}^2$ that appears in the second term, we can write this term as $\lambda_{m,n} D_{m,n}$, where $\lambda_{m,n}$ is the inertio-gravity wave frequency. If f is constant, $\lambda_{m,n} = \sqrt{k(k+1)c_n^2 + f^2}$, where k is the total wavenumber.

Define the geopotential $\phi = \gamma_r T + \sigma_r \ln p_{surf}$. Use a suffix n applied to the model variables to denote their projection on the nth vertical mode. The potential vorticity, Q, consistent with the linearisation (1) is then defined for each vertical normal mode by the equations

$$Q_n = c_n^2 \zeta_n - \mathbf{F}\phi_n \tag{4}$$

We can easily verify that this satisfies the equation

$$\frac{\partial Q_n}{\partial t} = c_n^2 E_n \mathcal{Z} - E_n(\gamma_r \mathcal{T} + \sigma_r \mathcal{P}), \tag{5}$$

so that the divergence is eliminated. A natural change of variables is then, following Bartello (1995), to use Q and R to replace vorticity and temperature and surface pressure, where R is the geostrophic departure defined as $\nabla^2(\gamma_r T + \sigma_r \ln p_{surf}) - \mathbf{F}\zeta$. The original variables can then be calculated from the transformed variables by solving for each vertical mode the equations:

$$\begin{aligned}(c_n^2 - \mathbf{F}\nabla^{-2}\mathbf{F})\zeta_n &= Q_n + \mathbf{F}\nabla^{-2}R_n \\ (\mathbf{F}^2 - c_n^2\nabla^2)\phi_n &= -(\mathbf{F}Q_n + c_n^2 R_n)\end{aligned} \tag{6}$$

T_n and $\ln p_{surfn}$ are then deduced from ϕ_n.

Equations (6) shows that for large vertical and small horizontal scales, where $c_n^2 \gg \mathbf{F}^2$, $c_n^{-2}Q_n \simeq \zeta_n$. In the opposite case $c_n^2 \ll \mathbf{F}^2$, we have $Q_n \simeq \mathbf{F}\phi_n$. Thus the potential vorticity is essentially vorticity on small horizontal and large vertical scales and essentially geopotential in the opposite case, in agreement with standard geostrophic adjustment theory, Haltiner and Williams (1980). Similarly, if $c_n^2 \gg \mathbf{F}^2$, $R_n \simeq \nabla^2\phi_n$ and if $c_n^2 \ll \mathbf{F}^2$, $R_n \simeq -\mathbf{F}\zeta_n$. Thus in the first case the imbalance, R_n, is primarily geopotential, and in the latter case it is primarily vorticity. If $c_n^2 \gg \mathbf{F}^2$, the vorticity will be primarily balanced and any imbalance will appear in the geopotential. If $c_n^2 \ll \mathbf{F}^2$, the geopotential will be primarily balanced and any imbalance will appear in the vorticity.

There is a basic difficulty with this procedure. The linear operator on the left hand side of the second equation is exactly the operator L with eigenvalues $\lambda_{m,n}$ that appears in equation (3). Equation (6) cannot be solved if either of the linear operators on the left hand side have a zero eigenvalue. This occurs for a particular meridional structure which is a zero eigenvalue of $\mathbf{F}^2$, Daley (1996), and for a vertical profile of T and $\ln p_s$ which gives a zero geopotential. The latter situation is possible on the Lorenz vertical grid, see Cullen et al. (1997). This vertical grid is used in most operational models, including the ECMWF model. The existence of the 'zero mode' prevents increments to ϕ being readily used to deduce increments to T and $\ln p_{surf}$. Furthermore, since during the assimilation the right hand side of (6) will contain increments generated statistically from the minimisation algorithm, there can be a significant projection onto small eigenvectors of the linear operators on the left-hand side. This is found to cause failure of the minimisation algorithm when this change of variable is used within the ECMWF 4D-VAR system.

The best solution found is to use as control variables 'balanced' vorticity ζ_b and 'unbalanced' temperature and surface pressure T_u and $\ln p_{surfu}$. The 'balanced' vorticity implies a balanced temperature and height through the linear balance relation. The 'unbalanced' temperature and surface pressure imply an unbalanced vorticity such that the potential vorticity calculated from the unbalanced variables is zero. For a single vertical mode, these variables are related to Q and R by the equations

$$\begin{aligned}(c_n^2 - \mathbf{F}\nabla^{-2}\mathbf{F})\zeta_{bn} &= Q_n \\ (\mathbf{F}^2 - c_n^2\nabla^2)\phi_{un} &= -c_n^2 R_n\end{aligned} \tag{7}$$

The transformations between these variables and the standard model variables for this mode are

$$\begin{aligned} \nabla^2\phi_{bn} &= \mathbf{F}\zeta_{bn} \\ T_n &= \tau_r c_n^{-2}\phi_{bn} + T_{un} \\ \ln p_{surfn} &= \nu_r c_n^{-2}\phi_{bn} + \ln p_{surfun} \\ \phi_{un} &= \gamma_r T_{un} + \sigma_r \ln p_{surfun} \\ \zeta_n &= c_n^{-2}\phi_{un} + \zeta_{bn} \end{aligned} \tag{8}$$

This choice avoids inverting the linear operators on the left hand side of (6) within the minimisation, though they still have to be inverted when converting model fields to control variables in the initial calibration procedure.

Even with the choice of control variables defined in (7), the change of variable was found unsatisfactory in assimilation experiments. In particular, vertical oscillations developed in the stratospheric temperature increments. The eigenfunctions corresponding to the smallest eigenvalues of the matrix **B** have a characteristic signal of vertical oscillations in the stratosphere. This is a characteristic feature of the Lorenz vertical staggering of variables, and can be resolved using the Charney-Phillips vertical staggering, Arakawa and Moorthi (1987), instead. Recently, Untch and Hortal (2002) have developed a vertical finite-element discretisation for the Lorenz grid which is less susceptible to vertical oscillations than the standard discretisation. The effect is illustrated in Fig.1. We see that the magnitude of the smallest gravity wave speeds is substantially increased over those given by the standard scheme. The values are intermediate between those given by standard finite-difference discretisation on the Lorenz and Charney-Phillips grids. The finite-element scheme was therefore used in the experiments described in this paper. It will be shown that the behaviour is then satisfactory but there is still some evidence of numerical problems which could only be properly resolved by using the Charney-Phillips grid.

The linear operators on the left hand side of (7) can be inverted successfully using the vertical finite-element scheme. However, the results shown in the next section show some evidence of numerical errors. We therefore add a value $10^{-10}\nabla^{-2}$ to each diagonal entry of the matrix $\mathbf{F}\nabla^{-2}\mathbf{F}$ on the left hand side of the first equation in (7). This reduces the magnitude of the balanced vorticity on small vertical and large horizontal scales. In order to preserve invertibility of the change of variable, the definitions of unbalanced temperature and surface pressure in (7) are replaced by $T_{un} = T_n - T_{bn}$ and $\ln p_{surfun} = \ln p_{surfn} - \ln p_{surfbn}$. The unbalanced vorticity is still defined by $\zeta_n = c_n^{-2}\phi_{un}$. The method of converting balanced geopotential to temperature and surface pressure ensures that $\gamma_r T_{bn} + \sigma_r \ln p_{surfbn} = \phi_{bn}$, so that the transformation from geopotential to temperature and surface pressure is invertible. Implicitly this makes a specific choice of how to handle the zero mode.

This regularisation improves the structure of the correlation matrices. However, it does not help the assimilation process, where the transformations are defined by (8). We show in the next section that there are convergence problems associated with small vertical scales. We address these by excluding some modes from (8) altogether. The change of variable is then replaced by the identity operator for these modes. For particular total wavenumbers and vertical modes we thus replace the second, third and fifth equation of (8) by

$$\begin{aligned} T_n &= T_{un} \\ \ln p_{surfn} &= \ln p_{surfun} \\ \zeta_n &= \zeta_{bn} \end{aligned} \tag{9}$$

The operational balance operator described by Bouttier et al. (1997) includes the generation of statistical correlations between vorticity and divergence. The temperature and surface pressure are correlated directly

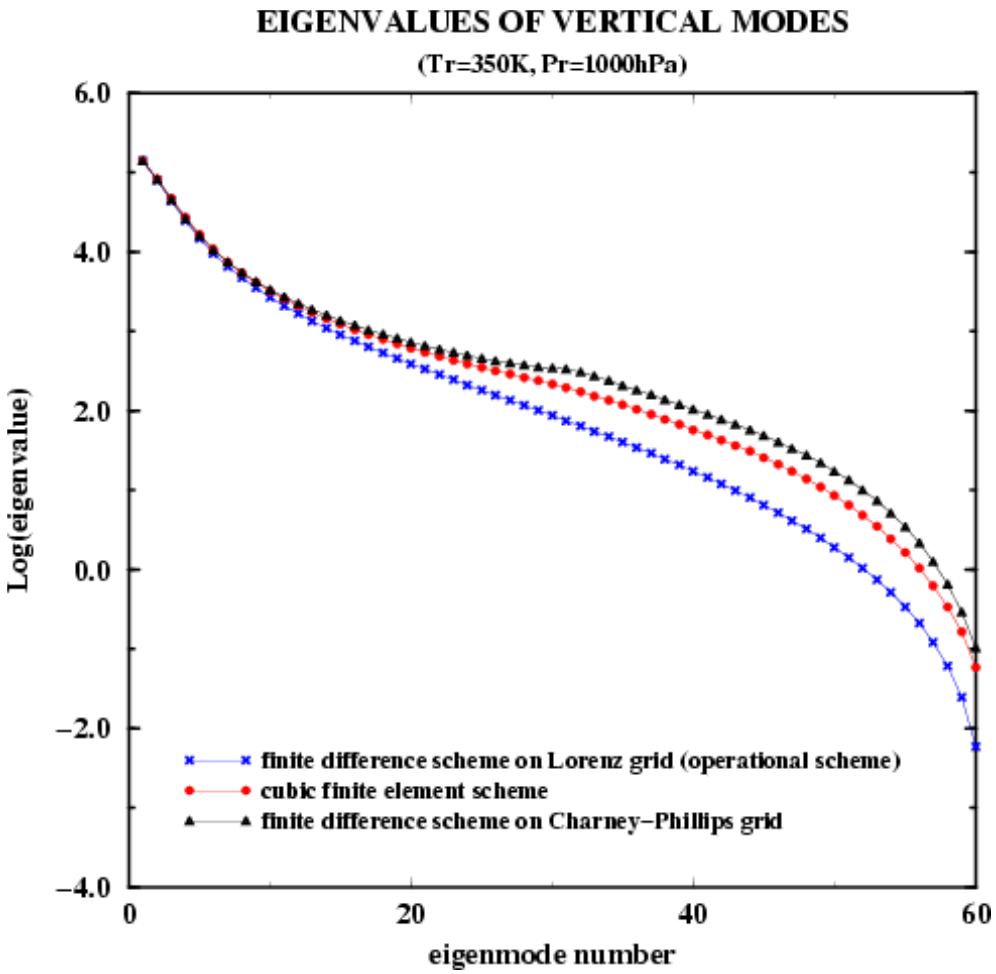

Figure 1: Values of the gravity wave speed expressed as $\log_{10} c_n^2$ for a 60-level version of the ECMWF model: (a) operational scheme on Lorenz staggering, (b) vertical cubic finite-element scheme, (c) Charney-Phillips staggering. Taken from Untch and Hortal (2002)

with the vorticity and the divergence, and the remainder treated as unbalanced. In our scheme, the change of variable from vorticity, temperature and surface pressure to balanced vorticity has to be performed analytically, and the zero mode problem solved as described above. In order to maintain the benefits of the other features of the operational balance operator, correlations are calculated statistically between balanced vorticity, divergence, humidity mixing ratio, and ozone. A statistical correlation is also calculated between the total vertical motion and the moisture and ozone. The remaining parts of the moisture and ozone are treated as unbalanced.

3 Diagnostics of the transformation

The change of variable defined in the previous section, including the regularisation of (6), was applied to a set of 216 differences between 6 hour forecasts obtained using an ensemble of analyses where the use of observations was perturbed, ECMWF (2000). The calculations were performed at T255 spectral resolution with 60 vertical levels. The overall split between balanced and unbalanced components of the forecast differences is summarised in Table 1, which is integrated over all wavenumbers. Since this total is weighted towards the larger number of high wavenumbers, the split for various low wavenumber groups is shown in Fig. 2. We show this split with and without the regularisation, since the latter acts mainly on low wavenumbers.

Table 1: Percentages of balanced and unbalanced variance for each model variable averaged over all wavenumbers, using regularised change of variable.

	Vorticity	Temperature	Surf. pressure
Balanced	92.3	25.3	30.9
Unbalanced	12.1	81.2	44.0

Note that the total explained temperature variance is 106%. This increases to 112% if the regularisation is not used. This is because the balanced and unbalanced temperature each contain vertical oscillations which add together to produce the actual, fairly smooth, profile. The oscillations are associated with small values of c_n^2.

Fig. 2 shows that the proportion of balanced vorticity increases with wavenumber, as expected from the discussion following (6). Table 1 shows that the total vorticity errors are primarily balanced. This is because a simple average over total wavenumber gives a strong weighting towards larger wavenumbers, and thus most of the errors satisfy the condition $c_n^2\nabla^2 \gg \mathbf{F}^2$. Similarly, the temperature errors become less balanced as the wavenumber increases, and the total over all wavenumbers is primarily unbalanced. The regularisation reduces the balanced component of both, as expected. After regularisation, the surface pressure errors have a similar degree of balance for all the low wavenumbers shown. Without regularisation, the degree of balance increases with wavenumber for low wavenumbers, which is not expected and is thus evidence of numerical problems.

When averaged over all wavenumbers, only about 0.1% of the variance of divergence, moisture, and ozone is explained by the balance operator. However, locally much higher proportions are explained, for instance 1.7% of the ozone variance in levels close to the tropopause and 3% of the moisture variance in the lower stratosphere.

3.1 Correlation structures

Figures 3 and 4 illustrate the correlation structures of the new variables. These are derived using the regularised version of (6). Fig.3 shows that the vertical correlations between adjacent levels are increased for large horizontal scales in vorticity. This is because the balanced vorticity is largely determined by geopotential at these scales, and the geopotential inherently has a greater vertical correlation. Fig.4 shows that the unbalanced

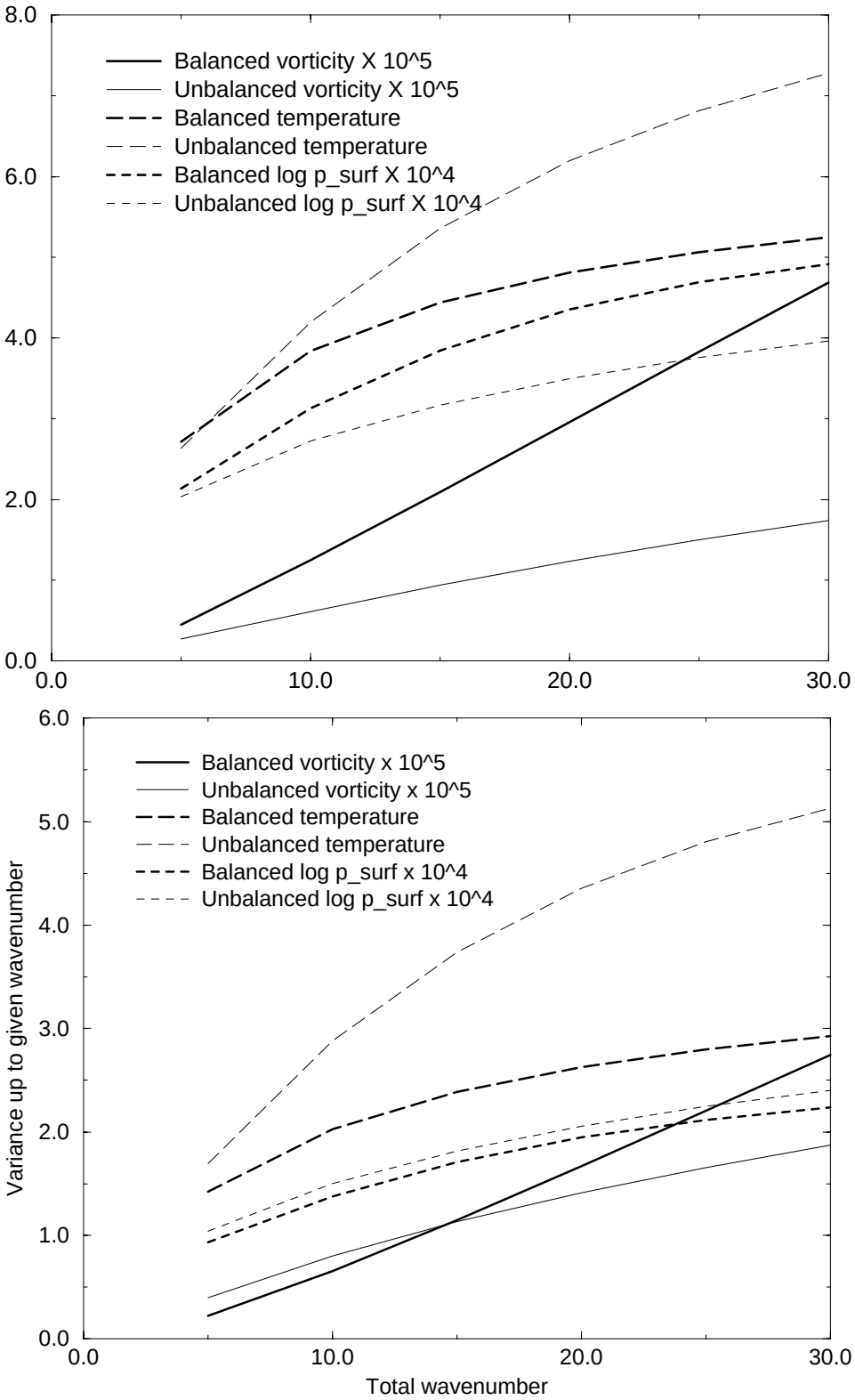

Figure 2: Standard deviation of balanced and unbalanced components of vorticity, temperature and logarithm of surface pressure in all wavenumbers up to given value. Data source as defined in text. Top picture-without regularisation. Bottom picture-with regularisation.

temperature correlations are much narrower in the horizontal. This is because the large-scale part of the temperature has moved into the balanced variable. If the regularisation is not used, the vertical correlation of balanced vorticity becomes small for the largest horizontal scales, suggesting that vertical oscillations are being created by the solution of (6).

4 Assimilation performance

4.1 Effect on the convergence of the minimisation

The new change of variable was tested in the ECMWF 4D-VAR scheme operational in early 2001 (CY23R4). The basic 4D-VAR configuration is set up as described by Mahfouf and Rabier (2000). The resolution used was T_L319 for the forecasts, with analysis increments calculated at T_L159. The operational 12-hour 4DVAR cycling was used. The control forecast additionally included the vertical finite-element scheme. The results shown are taken from a 35 day experiment for dates between June and July 2000. The regularised correlation matrices were used and the 5 highest vertical modes were excluded from the forecast error calculation in order to prevent instability of the error growth model. In the main experiment, no modes were excluded from the assimilation. Some results are included from an additional experiment in which the 5 highest vertical modes with total horizontal wavenumber less than or equal to 6 were excluded from the assimilation.

The rate of convergence of the minimisation in the forecast error calculation was calculated. This iteration is to convergence subject to a maximum of 150 iterations. The average reduction in gradient norm over 14 cycles was 0.149E-11 in the control, 0.90E-8 using the PV scheme, and 0.23E-8 using the PV scheme with some modes excluded. The reason for the poorer convergence rate in the PV scheme can be seen by looking at the eigenvalues of the Hessian, shown in Fig. 5. The figure shows the first 30 eigenvalues, each of which is averaged over the same 14 cycles. There are large variations of the magnitude of the eigenvalues from cycle to cycle, depending on the availability of observations. The eigenvalues in the PV scheme are larger, and thus the condition number is worse. The ratio of the largest to the smallest eigenvalue of the operator on the left hand side of (7) is about $5.5_{10}8$ using T_L159 resolution and the vertical finite-element scheme with 60 levels. This is to some extent reflected in the eigenstructure of the Hessian. The structure of the eigenfunction associated with the largest eigenvalue in one of the cycles is shown in Fig.6. It is essentially that of the mode with the smallest inertio-gravity wave speed $\lambda_{m,n}$.

Exclusion of some modes improves the eigenvalue structure, as shown in Fig.5, and also the convergence rate. It may also be possible to improve the convergence rate by preconditioning in either case, since there are only a few large eigenvalues. However, the analysis will still concentrate on analysing the structure represented by the largest eigenvalue, which may not be desirable.

4.2 Effect on the fit to observations

The implied background error zonal mean cross-sections are shown in Figs. 7 and 8 for one cycle 15 days into the experiment. The vorticity errors have higher values below the tropopause in the control experiment. The temperature background error has a strong variation with latitude using the PV variable, reflecting that a given vorticity error will imply a much smaller temperature error in the tropics than elsewhere. Even in the zonal mean, the error is noisy in the vertical. This comes from the inversion of vorticity into temperature through the linear balance relation and the difficult inversion from geopotential to temperature on the model grid.

Fig. 9 shows a zonal mean cross-section of the vorticity increments from one cycle. The cross-section is

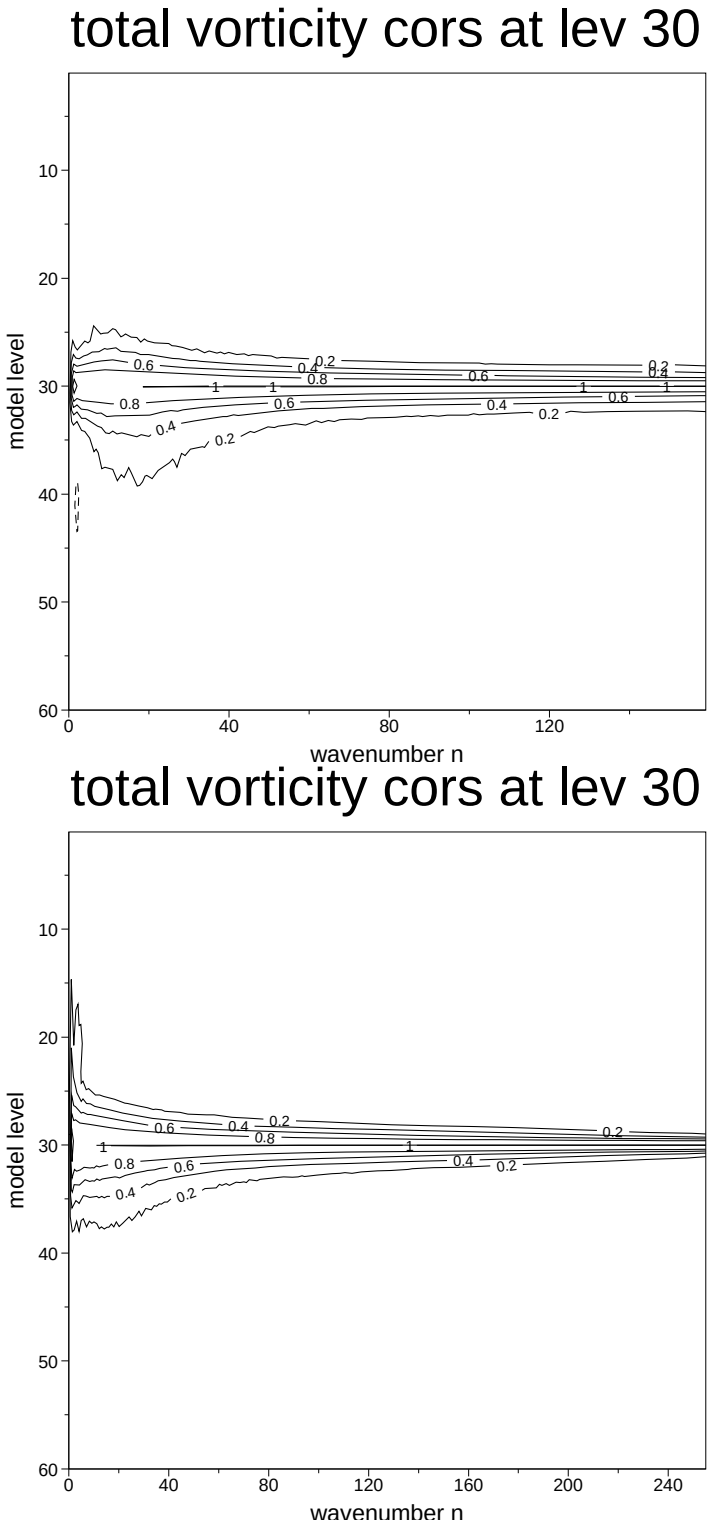

Figure 3: Correlation between balanced vorticity errors at model levels with the balanced vorticity error at model level 30 (250hpa). The correlations are plotted against total wavenumber. Top-control, bottom-PV scheme. Data source as defined in text.

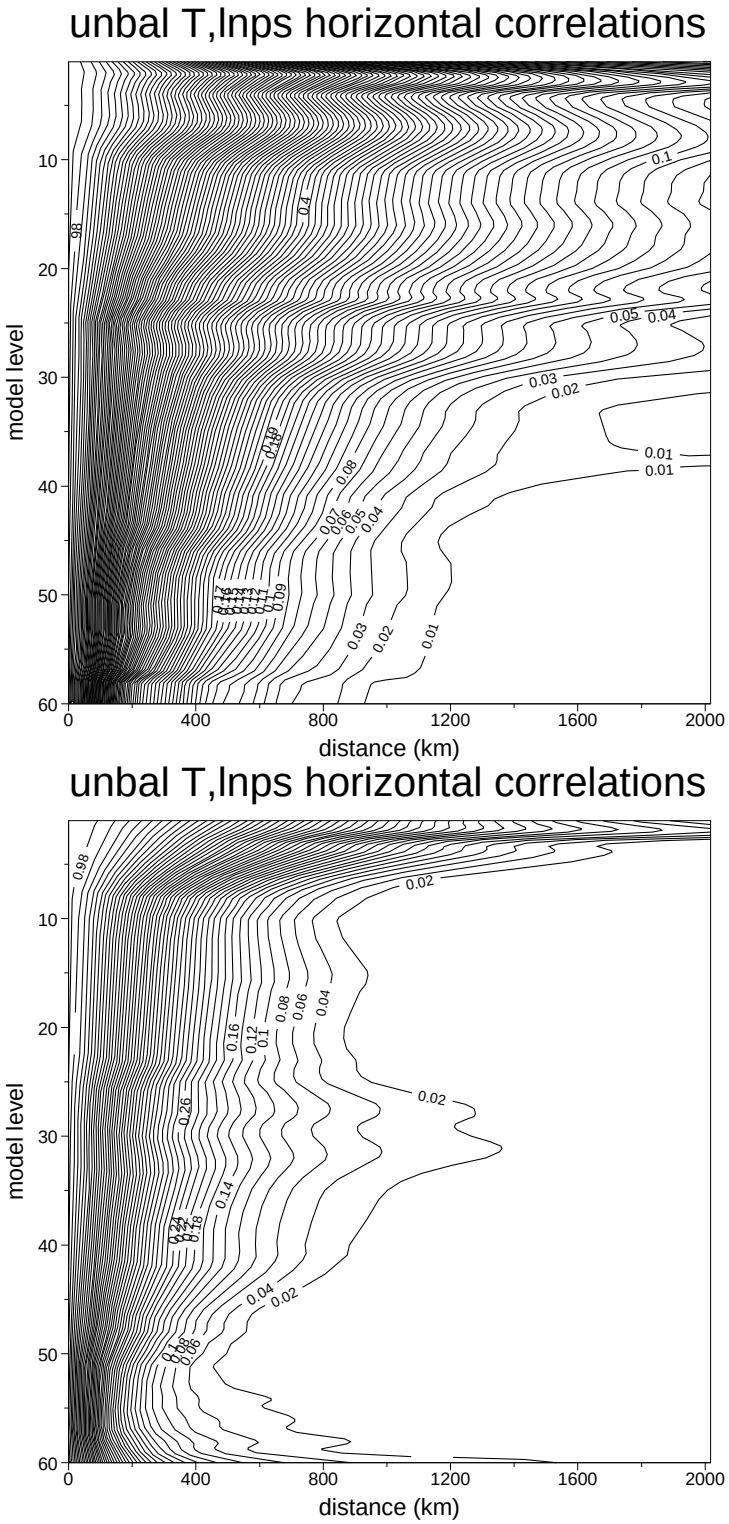

Figure 4: Unbalanced horizontal temperature error correlations averaged over all wavenumbers plotted against model level. Top-control, bottom-PV scheme. Data source as defined in text.

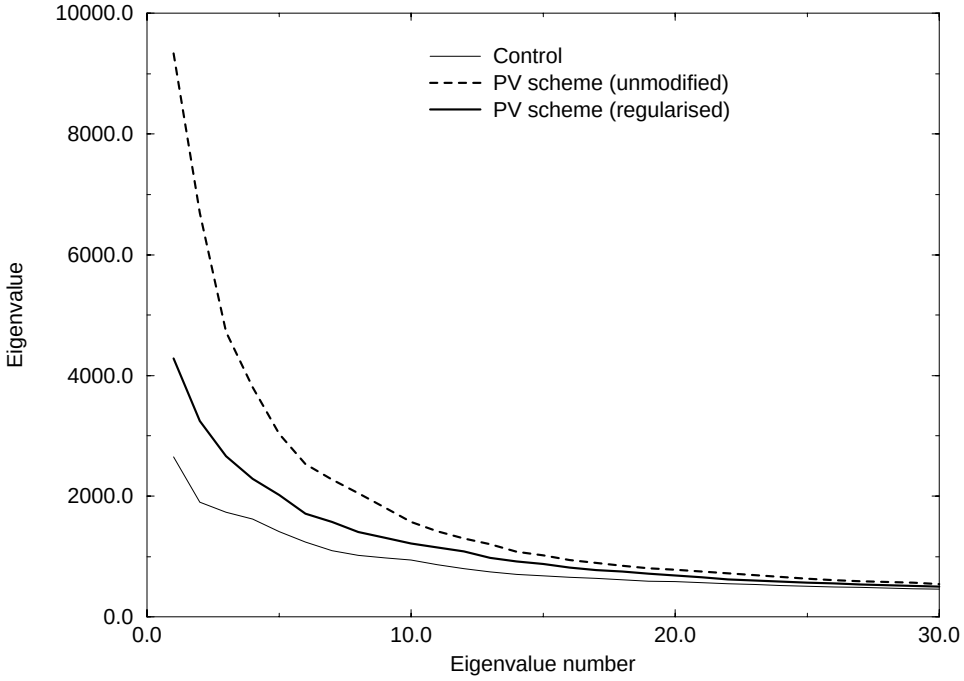

Figure 5: Average values of the first 30 eigenvalues of the Hessian computed over 13 assimilation cycles.

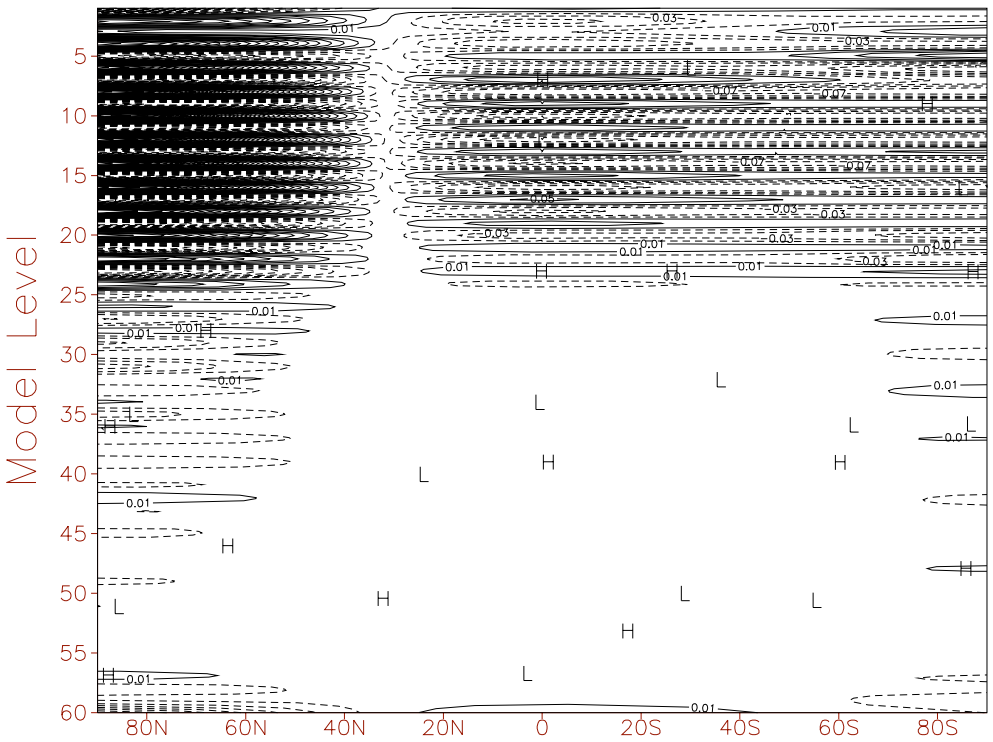

Figure 6: Zonal mean temperature cross-section (°K) of the eigenvector of the Hessian associated with the leading eigenvalue in one case.

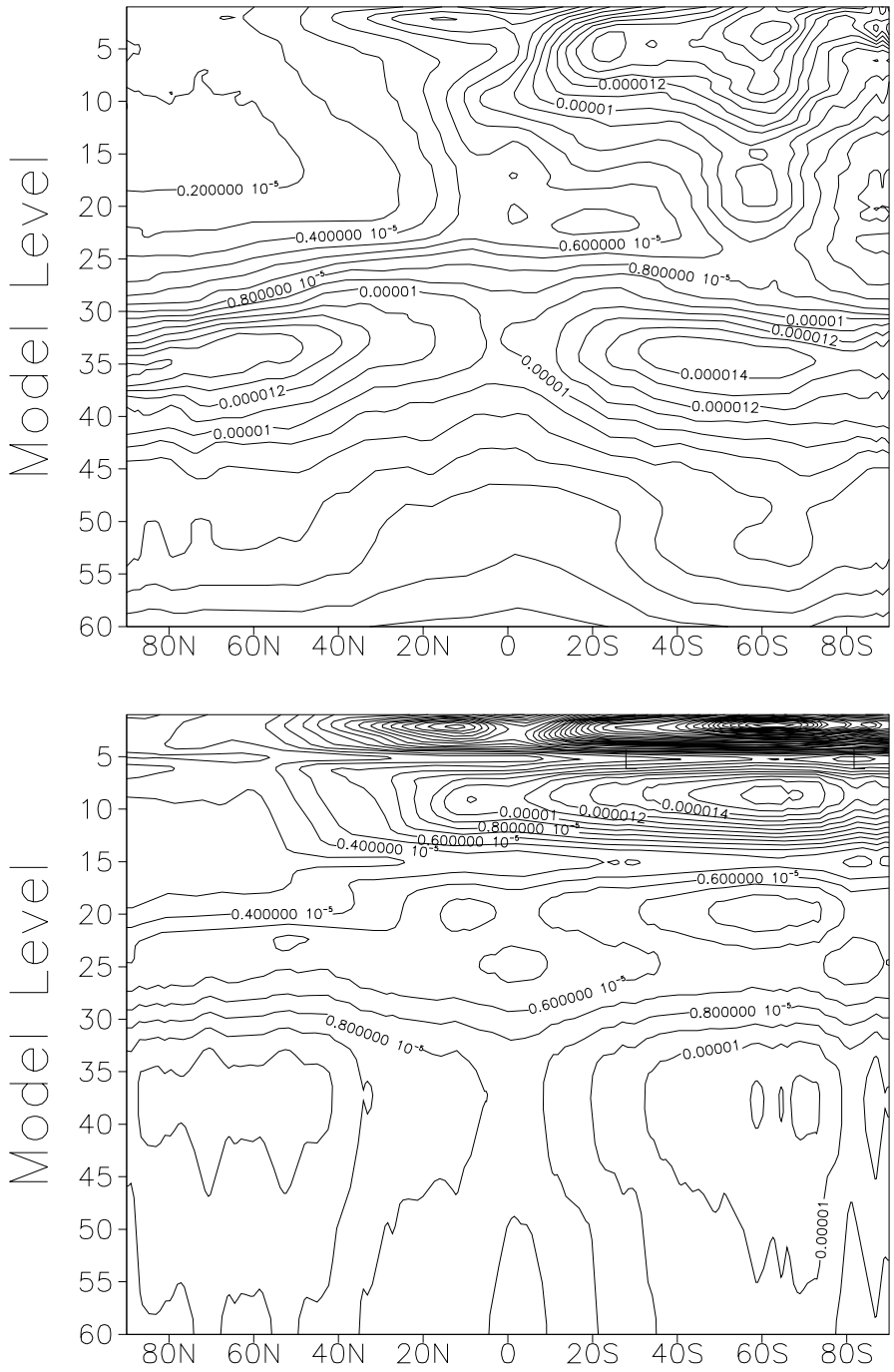

Figure 7: Zonal mean cross-section of the assumed background error (s^{-1})for vorticity for 1 July 2000. Top-control, bottom-PV scheme.

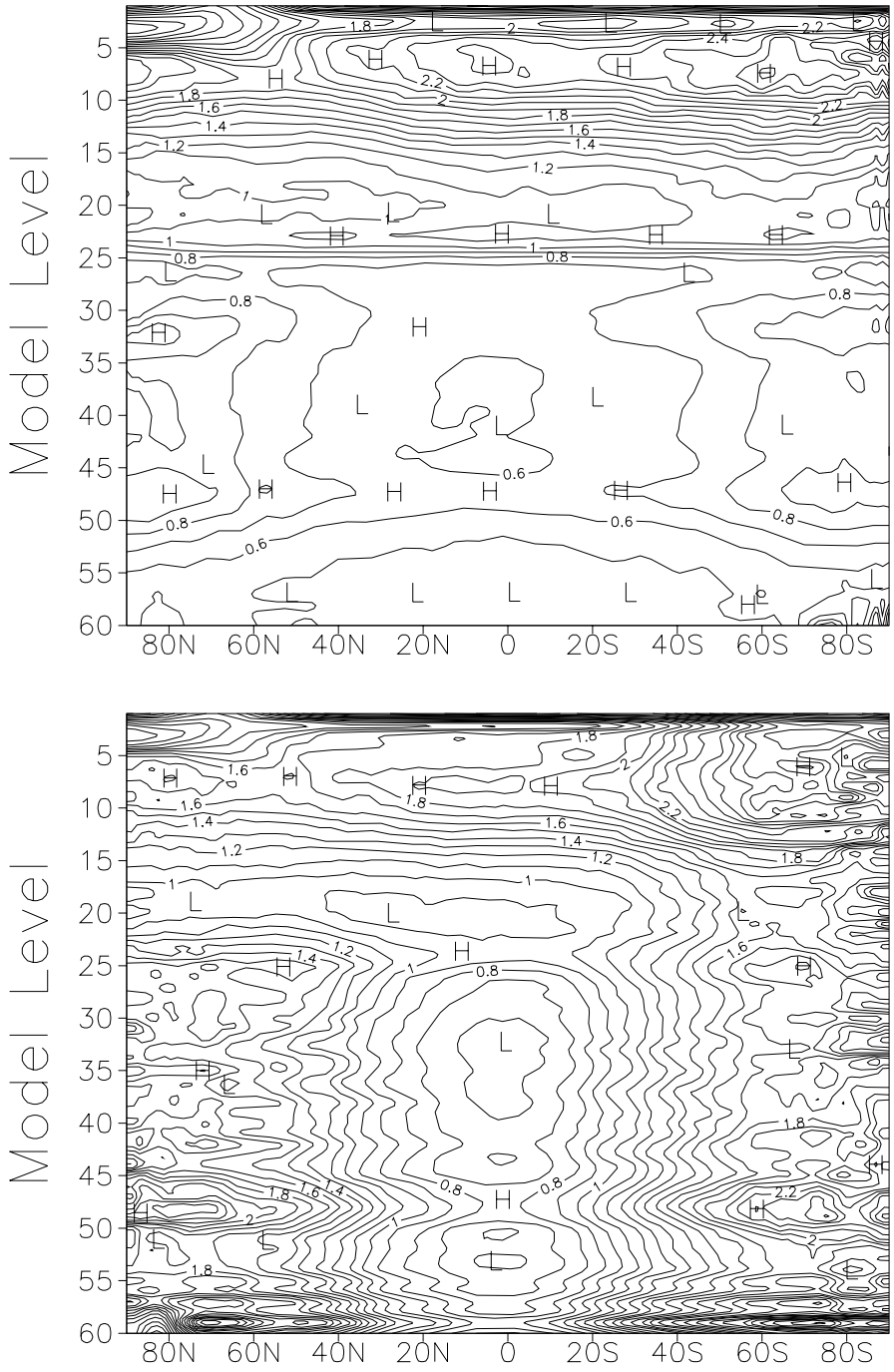

Figure 8: Zonal mean cross-section of the assumed background error for temperature (°K) for 1 July 2000. Top-control, bottom-PV scheme.

through the levels where the correlations of balanced vorticity shown in Fig. 3 are markedly broader in the PV scheme. The increments are smoother in the vertical in the tropics, but there is no systematic difference in the extra-tropics. Fig. 10 shows the equivalent temperature increments. The two experiments are similar in the tropics and sub-tropics. In high latitudes, the increments from the PV scheme have a tendency for vertical oscillations. The structure reflects that of the eigenmode shown in Fig. 6.

Figs. 11 and 12 show the effects on assimilation of radiosonde data. The short range forecast wind errors from the two experiments are similar, but slightly reduced in the PV scheme at the highest levels. The PV analysis draws less closely to wind data in the tropics, and slightly less closely in the Southern hemisphere. The short range temperature errors are similar except in the Southern hemisphere where those from the PV scheme are slightly larger. The PV analysis, however, draws as closely to the data in the Southern hemisphere and slightly closer in the Northern hemisphere. It draws less closely in the tropics. Almost identical results were obtained from the experiment with some modes excluded from the assimilation.

4.3 Effect on forecast performance

We illustrate the effect on forecasts by showing anomaly correlations and r.m.s errors for all 35 cases in the experiment. The model used was cycle 23R4 of the ECMWF model, with forecast resolution T319 and analysis increments calculated at T159. The operational 12-hour 4DVAR cycling was used. The control forecast additionally included the vertical finite-element scheme. Both sets of forecasts were verified against analyses produced from their own assimilation cycle.

Fig.13 shows a positive impact on medium-range performance in the Northern hemisphere extra-tropics and a negative impact in the Southern hemisphere extra-tropics. Similar results are obtained at other levels. There is a slightly negative impact on shorter range forecasts. There is a large spread of results from case to case, so the differences are generally only significant at the 10% level. There is a large impact on analyses and forecasts of winds in the tropics and upper stratosphere. Fig. 14 shows a large positive impact in the wind forecasts at 850hpa in the tropics, while the extra-tropical wind performance is similar to the geopotential shown in Fig.13. Similar impacts are seen at other levels. The impact on winds is only seen when the forecasts are measured against their own analyses, showing that the analyses have changed significantly. Verification against observations gives approximately equal scores for tropical wind forecasts from the two experiments. There is also a large positive impact (not shown) on the 50hpa wind errors in the extra-tropics as well as the tropics.

The difference in the wind verification figures are largest at upper levels. They can be understood by looking at a typical cross-section of a tropical wind analysis in the upper troposphere and lower stratosphere. The analysis using the potential vorticity scheme (Fig.15 middle) is substantially smoother. Given that the verification against observations is similar, the likelihood is that the balance of the assimilation has been improved, and fewer gravity waves are excited.

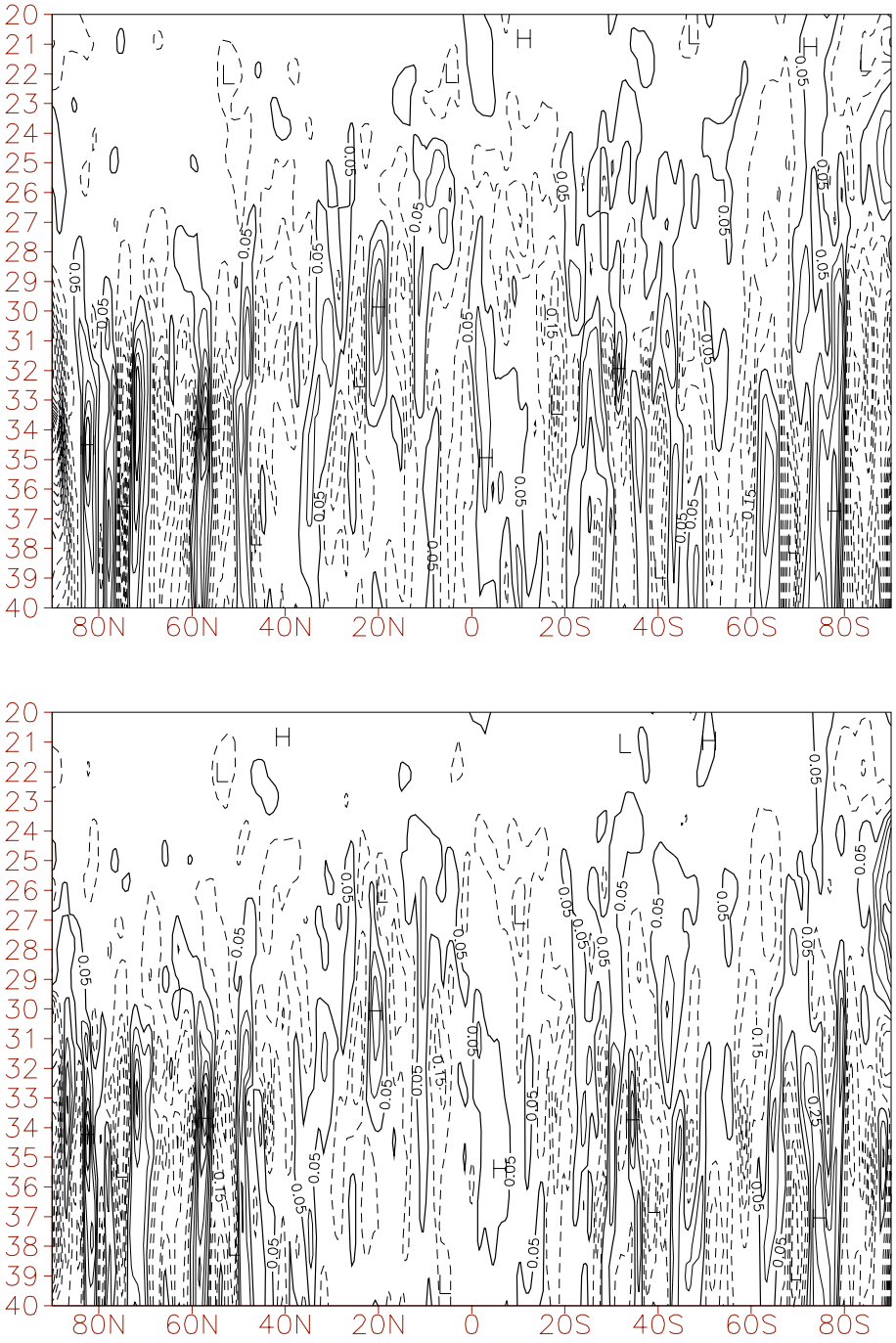

Figure 9: Zonal mean cross-section of vorticity increments between model levels 20 and 40 (approximately 30hpa to 500hpa) for the 12UTC cycle on 1 July 2000. Units $10^{-}5s^{-1}$. Top-control, bottom-PV scheme.

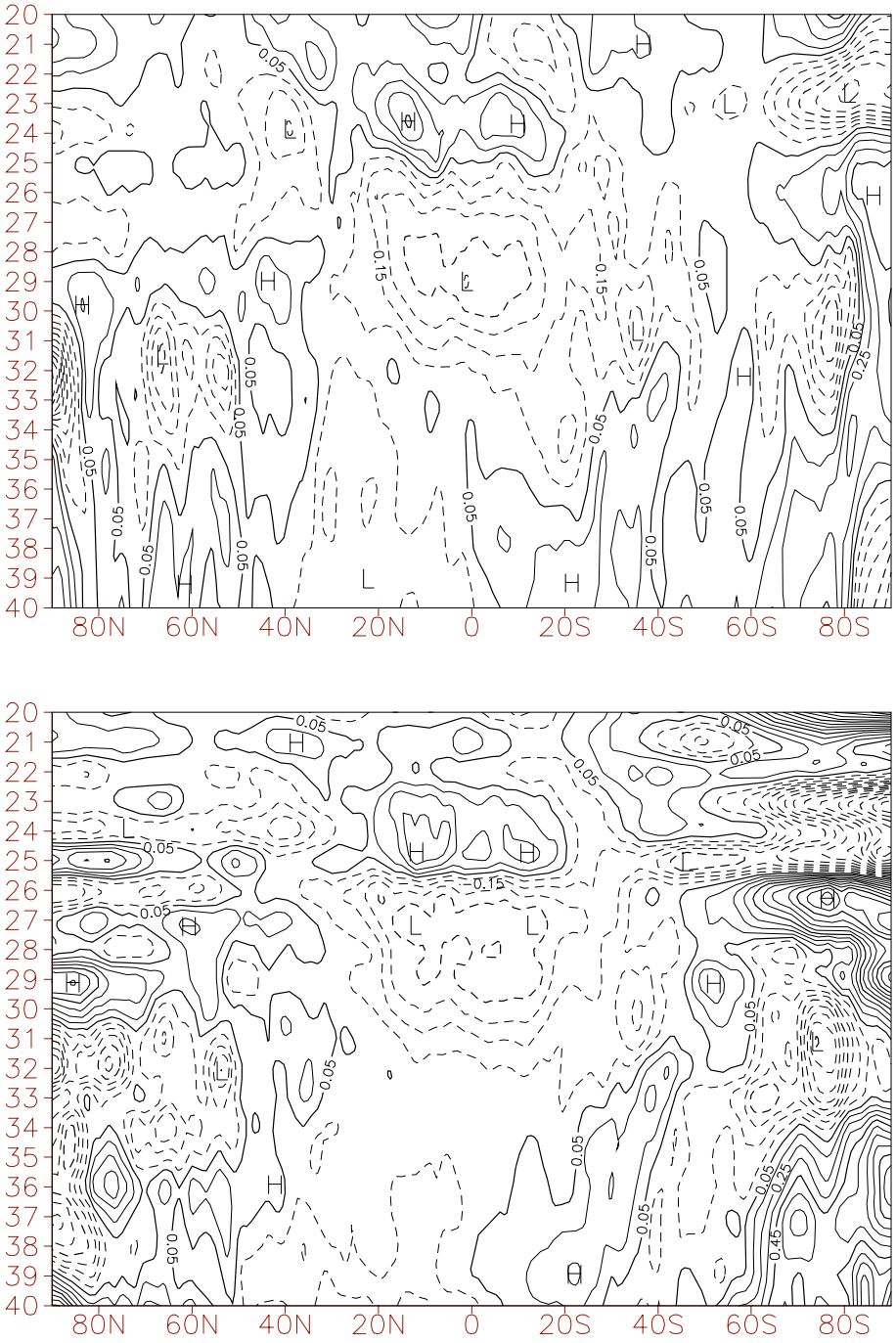

Figure 10: Zonal mean cross-section of temperature increments between model levels 20 and 40 for 1 July 2000. Units °K. Top-control, bottom-PV scheme.

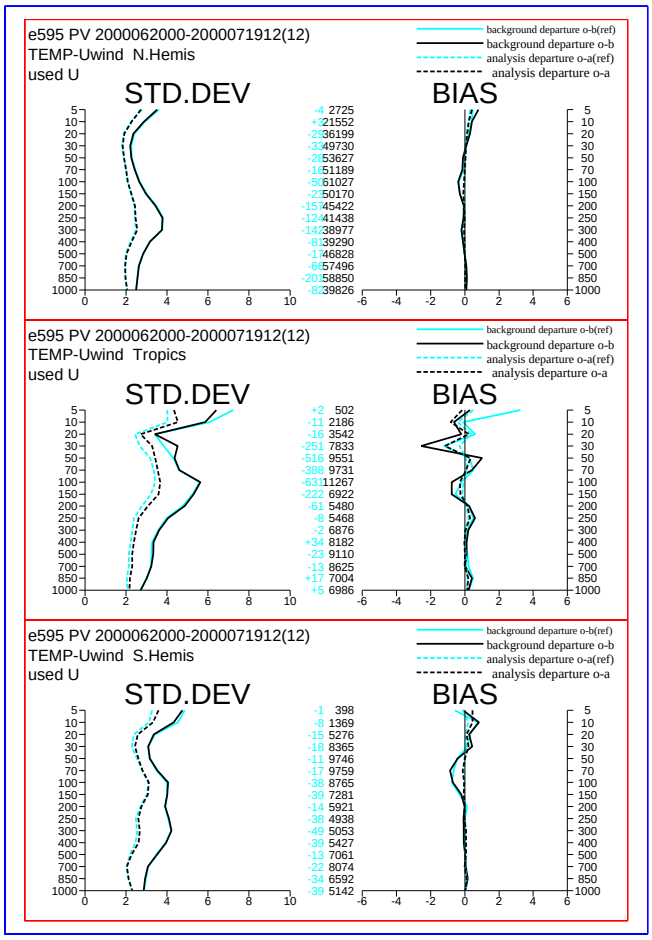

Figure 11: Observation minus background and observation minus analysis differences for the zonal component of the wind measured by radiosonde data averaged over all assimilation cycles from 20 June to 19 July 2000. Heavy lines, PV scheme; lighter lines, control.

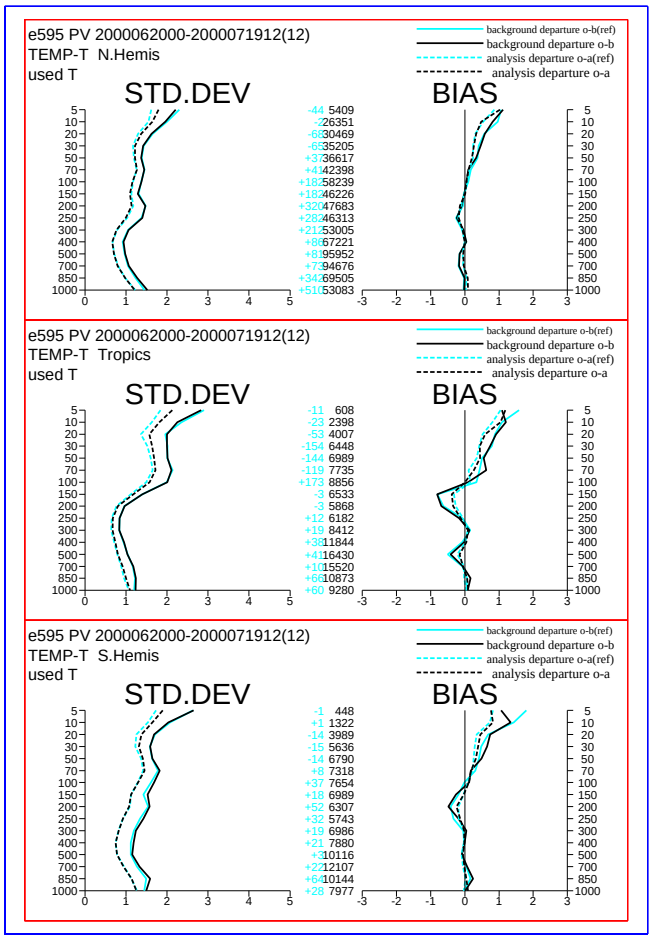

Figure 12: Observation minus background and observation minus analysis differences for the temperature measured by radiosonde data, notation and dates as Fig. 11.

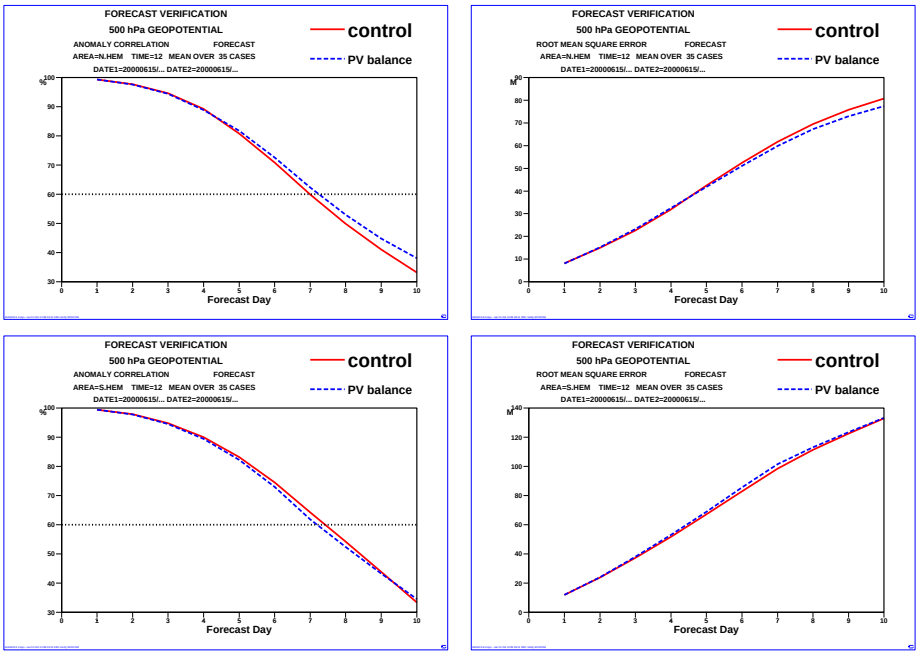

Figure 13: Anomaly correlations (percent) and r.m.s. errors (m) of 500hpa height for 35 test cases. Potential vorticity scheme plotted against the control. Both verifications are against own analyses

5 Discussion

The results illustrate that a balance operator based on potential vorticity can be used successfully in an operational model. Standard theory indicates that this should be the best way of defining such an operator. However, the use of such an operator is numerically difficult because of the large scale dependence of the internal gravity wave speed, and the use of the Lorenz vertical staggering. The results suggest that the impact is largest in the wind analysis in regions, such as the tropics and upper stratosphere, where the balance constraint should probably be weakest. The temperature analysis increments are more noisy, reflecting the attempt by the analysis to take the detailed vertical structure from temperature observations. The vertical grid makes this difficult, even with the use of the finite element discretisation. The difference between this scheme and the operational scheme is that it is possible to have an unbalanced vorticity increment, and that the use of an analytic change of variable enforces constraints much more strongly than the statistical method used in the operational scheme. The latter can give a more effective balance constraint, though at the price of numerical problems and a slower convergence rate in the assimilation.

Acknowledgements

The author wishes to thank many colleagues at ECMWF, particularly Mike Fisher, who taught the author how the data assimilation system worked, and provided extensive advice throughout, and Francois Bouttier, who provided the initial encouragement.

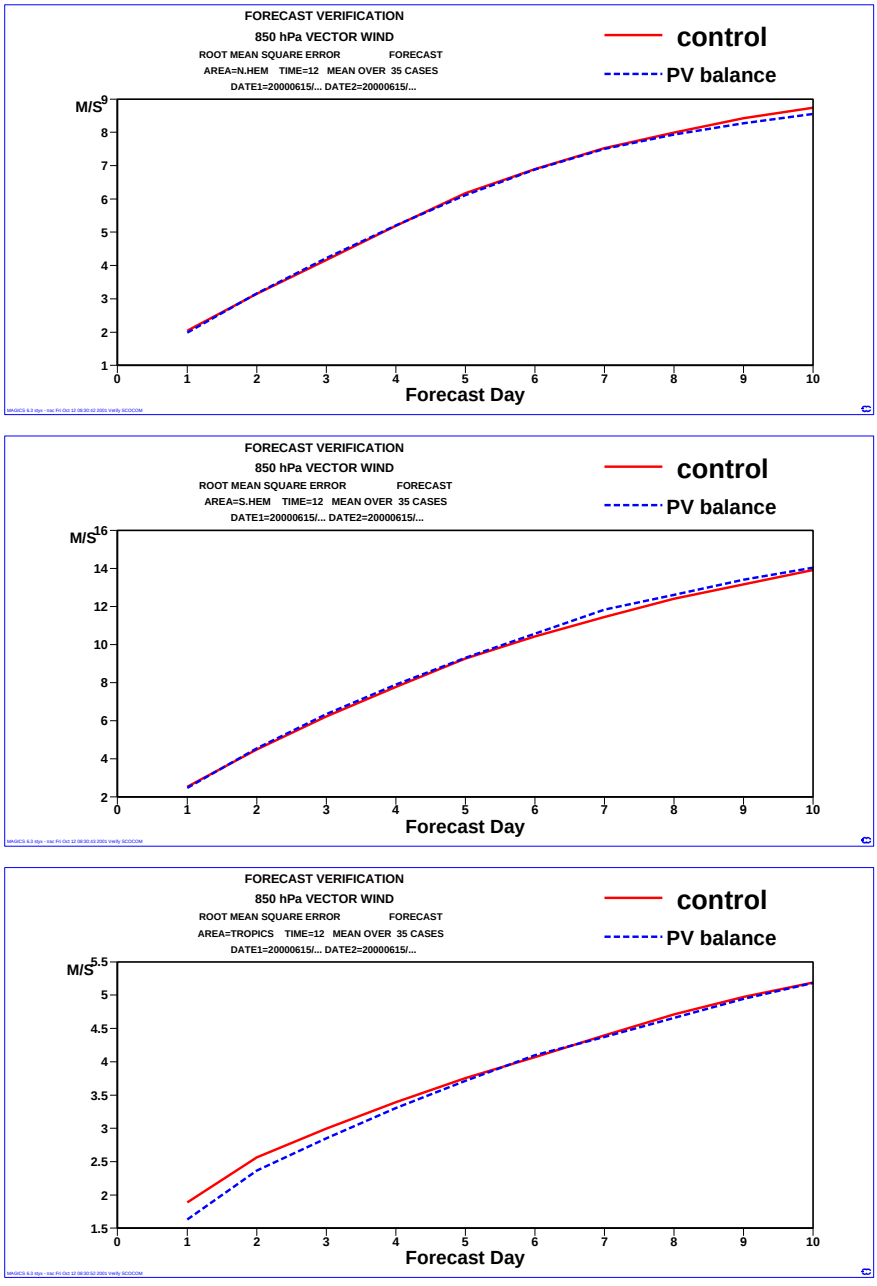

Figure 14: r.m.s. errors (m) of 850hpa winds for cases shown in Fig.11. Potential vorticity scheme plotted against the control, with verification against own analyses.

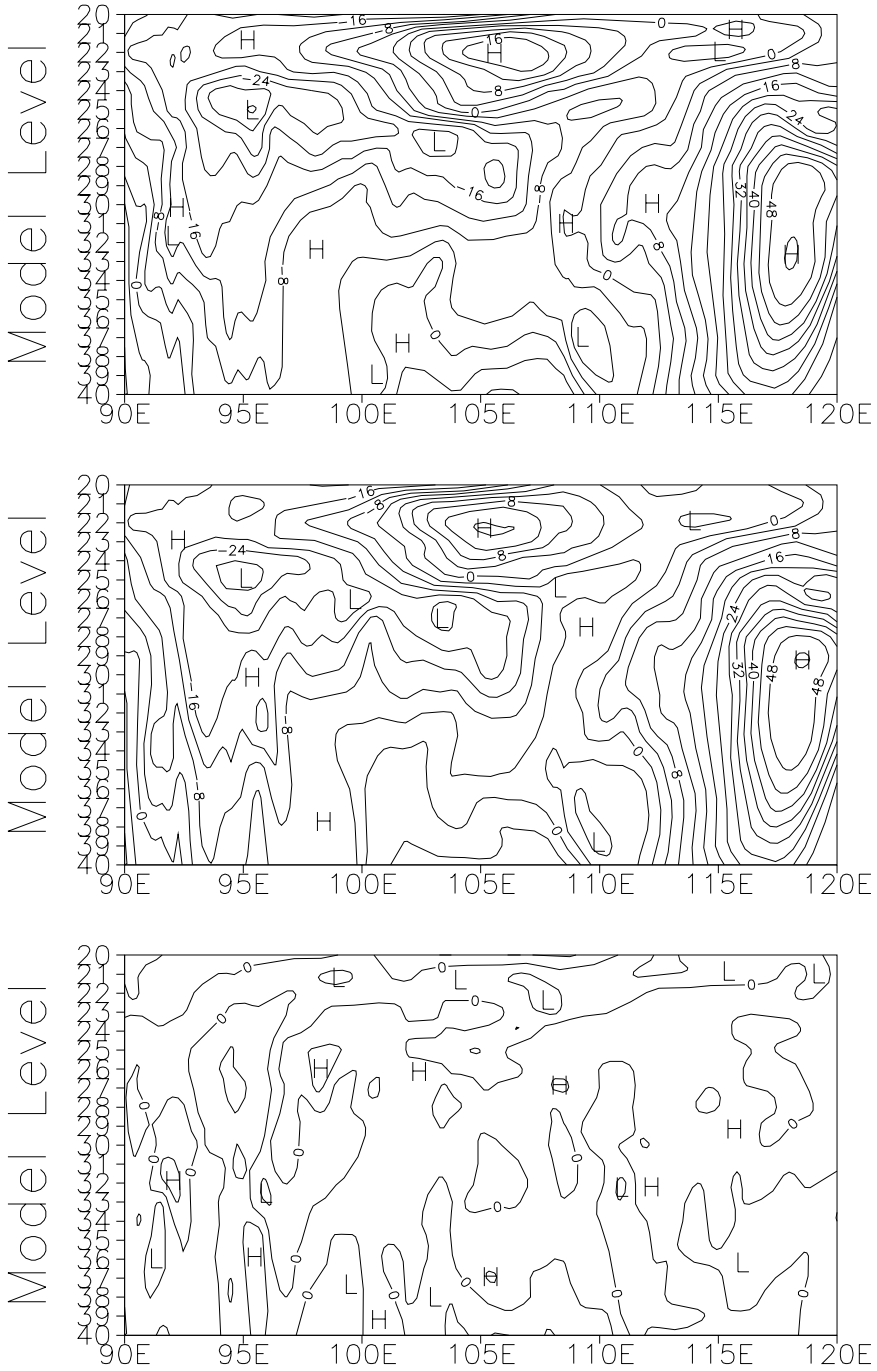

Figure 15: Cross-sections of analysed wind at model levels 20 to 40 (approximately 30-500hpa) between 30 $^{\circ}N$90 $^{\circ}E$ and 30 $^{\circ}S$120 $^{\circ}E$ for 12UTC on 1st July 2000. Top: control, middle: potential vorticity scheme, bottom: difference PV scheme-control.

References

Arakawa,A. and Moorthi,S. (1987): Baroclinic instability in vertically discrete systems; *J. Atmos. Sci.*, **45**, 1688-1707.

Bartello,P. (1995): Geostrophic adjustment and inverse cascades in rotating stratified turbulence; *J. Atmos. Sci.*, **52**, 4410-4428

Bouttier,F., Derber.J. and Fisher,M. (1997): The 1997 revision of the J_b term in 3D/4D-Var; *ECMWF Tech. Memo..*, no. 238.

Cullen,M.J.P., Davies,T., Mawson,M.H., James,J.A. and Coulter,S. (1997): An overview of numerical methods for the next generation UK NWP and climate model; in 'Numerical Methods in Atmosphere and Ocean Modelling', The Andre Robert Memorial Volume. (C.Lin, R.Laprise, H.Ritchie, Eds.), Canadian Meteorological and Oceanographic Society, Ottawa, Canada, 425-444.

Daley,R. (1996): Generation of global multivariate error covariances by singular-value decomposition of the linear balance equation; *Mon. Weather Rev.* **124** 2574-2587.

ECMWF (2000): The IFS cycle CY21r4 made operational in October 1999; *ECMWF Newsletter*, no. 87, 24pp.

Haltiner, G.J. and Williams,R.T. (1980) *Numerical prediction and Dynamic Meteorology,* 2nd ed. John Wiley and Sons., 477pp.

Mahfouf,J.-F. and Rabier,F. (2000): The ECMWF operational implementation of four-dimensional variational data assimilation. II: Experimental results with improved physics; *Quart. J. Roy. Meteor. Soc.*, **126**, 1143-1170.

Parrish,D.F. and Derber,J.C. (1992): The National Meteorological Center's spectral statistical interpolation analysis system: *Mon. Weather Rev.*, **120**, 1747-1763.

Rabier,F., Jarvinen,H., Klinker,E., Mahfouf,J.-F. and Simmons,A.J. (2000): The ECMWF operational implementation of four-dimensional variational data assimilation. I: Experimental results with simplified physics; *Quart. J. Roy. Meteor. Soc.*, **126**, 1143-1170.

Simmons,A.J. and Temperton,C. (1997): Stability of a two-time-level semi-implicit integration scheme for gravity wave motion; *Mon. Weather Rev.*, **125**, 600-615.

Temperton,C. (1997): Treatment of the Coriolis terms in semi-Lagrangian spectral models; in 'Numerical Methods in Atmosphere and Ocean Modelling', The Andre Robert Memorial Volume. (C.Lin, R.Laprise, H.Ritchie, Eds.), Canadian Meteorological and Oceanographic Society, Ottawa, Canada, 279-292.

Untch,A. and Hortal,M. (2002): A finite element scheme for the vertical discretisation in the semi-Lagrangian version of the ECMWF forecast model; (in preparation).